Journal Pre-proofs

Design and synthesis of β-strand-fixed peptides inhibiting aggregation of amyloid β-protein

Fumiya Tanaka, Kana Shibata, Yoko Monobe, Ken-ichi Akagi, Yuichi Masuda

PII: S0968-0896(20)30506-X
DOI: https://doi.org/10.1016/j.bmc.2020.115676
Reference: BMC 115676

To appear in: *Bioorganic & Medicinal Chemistry*

Received Date: 22 May 2020
Revised Date: 13 July 2020
Accepted Date: 17 July 2020

Please cite this article as: Tanaka, F., Shibata, K., Monobe, Y., Akagi, K-i., Masuda, Y., Design and synthesis of β-strand-fixed peptides inhibiting aggregation of amyloid β-protein, *Bioorganic & Medicinal Chemistry* (2020), doi: https://doi.org/10.1016/j.bmc.2020.115676

Design and synthesis of β-strand-fixed peptides inhibiting aggregation of amyloid β-protein

Fumiya Tanaka[a], Kana Shibata[a], Yoko Monobe[b,1], Ken-ichi Akagi[b,2], and Yuichi Masuda[a,*]

[a]*Graduate School of Bioresources, Mie University, 1577 Kurimamachiya-cho, Tsu, 514-8507, Japan*

[b]*National Institute of Biomedical Innovation, Health and Nutrition, Osaka 567-0085, Japan*

*Corresponding author: Tel.: +81-59-231-9620; E-mail: masuda@bio.mie-u.ac.jp

Present Addresses

[1]*Hanaichi UltraStructure Research Institute, Co., Ltd. 36 Teramae, Ida-cho-aza, Okazaki, Aichi, 444-0076, Japan*

[2]*Environmental Metabolic Analysis Research Team, RIKEN Center for Sustainable Resource Science, Yokohama, Kanagawa 230-0045, Japan*

Abstract

Aggregation of 42-residue amyloid β-protein (Aβ42) can be prevented by β-sheet breaker peptides (BSBps) homologous to LVFFA residues, which are included in a β-sheet region of Aβ42 aggregates. To enhance the affinity of BSBps to the Aβ42 aggregates, we designed and synthesized β-strand-fixed peptides (BSFps) whose side chains were cross-linked by ring closing metathesis. Conformation analysis verified that the designed peptides could be fixed in β-strand conformation. Among the synthesized pentapeptides, **1** and **12**, whose side chains of 2nd and 4th residues were cross-linked, significantly inhibited the aggregation of Aβ42. This suggested that β-strand-fixation of BSBps could enhance their inhibitory activity against the Aβ42 aggregation. However, pentapeptides **1** and **12** had little effect on morphology of Aβ42 aggregates (fibrils) and neurotoxicity of Aβ42 against SH-SY5Y cells.

Keywords:

Amyloid β-protein, β-sheet breaker peptide, β-strand mimetics, conformation fixation, conformation analysis

Abbreviations

AD, Alzheimer's disease; Aβ, amyloid β-proteins; BSBp, β-sheet breaker peptide; BBB, blood-brain barrier; Tyr(Allyl), *O*-allyl-tyrosine; Gly(Allyl), allylglycine; BSFp, β-strand-fixed peptides; HBTU, [Bis(dimethylamino)methylene]-1*H*-benzotriazolium 3-Oxide Hexafluorophosphate; DIEA, *N,N*-diisopropylethylamine; RCM, ring-closing metathesis; DMSO, dimethyl sulfoxide; NOE, nuclear Overhauser effect; Th-T, thioflavin-T, TEM, transmission electron microscopy; MTT, 3-(4,5-dimethylthiazol-2-yl)-2,5-diphenyltetrazolium bromide; RP-HPLC, reversed-phase high performance liquid chromatography; HFIP, 1,1,1,3,3,3-hexafluoro-2-propanol; PBS, phosphate buffered saline

1. Introduction

Alzheimer's disease (AD), the leading cause of dementia, is neuropathologically characterized by appearance of senile plaques in the cerebral cortex.[1] Senile plaques are mainly composed of aggregated 40- and 42-mer amyloid β-proteins, called Aβ40 and Aβ42, respectively (Figure 1A).[2, 3] After excised from amyloid precursor protein, Aβ forms intermolecular β-sheets to aggregate. Aggregation of Aβ induces neurotoxicity,[4] which is thought to be the main cause of AD. Since Aβ42 is far more aggregative than Aβ40,[5] inhibition of Aβ42 aggregation is expected to be an effective treatment for AD.

The structure of the Aβ42 aggregates (fibrils) has been intensively studied to elucidate the aggregation mechanism.[6, 7] The Aβ42 aggregates were revealed to form intermolecular parallel β-sheets, in which β-strands (a 'β-strand' is a stretch of amino acids whose peptide backbones are almost fully extended) are connected with intermolecular hydrogen bonds.[8-10] Hydrophobic residues at the positions 17−21 (LVFFA) of Aβ42 are considered to play critical roles in the aggregation by forming a core β-sheet structure in the central region (Figure 1A). In addition, intermolecular π–π stacking of two successive phenylalanines at the positions 19 and 20 might help the parallel alignment of β-strands.[11, 12] The aggregation of Aβ42 can be hampered in the presence of short peptides homologous to the 'LVFFA' residues (known as β-sheet breaker peptide, BSBp). Soto *et al.* first synthesized a series of BSBps and developed a famous BSBp called iAβ5 (LPFFD).[13, 14] So far, many researchers have developed BSBp with good inhibitory activity against the Aβ aggregation *in vitro*.[15, 16] However, the peptide backbones should be susceptible to proteolytic degradation and hard to cross the blood-brain barrier (BBB). To overcome these problems, BSBps have been subjected to various chemical modifications, such as *N*-methylation[17, 18] and incorporation of unnatural amino acids including D-isomers.[19, 20] These modifications could improve their biological stability and BBB permeability, showing a great potential of BSBp for becoming a drug for AD.

Although a variety of BSBps have been developed, their inhibitory activities were not sufficient for practical use. In general, to enhance the affinity of the ligands to their target proteins, it is necessary to consider enthalpic as well as entropic contribution. In case of BSBp, conformation fixation of BSBp to a β-strand conformation would be a good approach for reducing the entropy loss upon binding. Arai *et al.* designed and synthesized cyclic BSBps to identify the pharmacophores by stabilizing the active conformation.[21, 22] Quite recently, Jha *et al.* reported a promising example of a conformationally restricted BSBp.[23] They developed an octapeptide with a β-hairpin structure stabilized by a β-turn-inducing segment (^{D}Pro-Gly motif) and a disulfide cross-linkage. The β-hairpin-containing peptide was found to inhibit the aggregation and neurotoxicity of Aβ42. This report demonstrated that the conformation-fixation could be a powerful approach for enhancing the inhibitory activity of BSBp.

The molecular size of BSBps should be as small as possible to keep the good BBB permeability for AD drug. Although many methods for β-strand-fixation of the peptide backbone have been proposed,[24, 25] a compact motif of a β-strand is preferred for the design of conformation-fixed BSBp. Abell *et al.* designed and synthesized a tripeptide, in which, the side chains of the 1st and 3rd residues (*O*-allyl-tyrosine (Tyr(Allyl)) and allylglycine (Gly(Allyl)), respectively) were cross-linked with (*E*)-alkene by ring-closing metathesis (RCM) (Figure 1B).[26, 27] X-ray crystal analysis of the synthesized peptide revealed its β-strand geometry (Figure 1C).[27] Abell *et al.* also reported that β-strand fixation of the peptides could enhance their inhibitory activity against the calcium-activated cysteine protease calpain.[26] It is noteworthy that Abell's motif can fix the peptide conformation in a β-strand without increasing its molecular size. Moreover, this motif includes an aromatic ring, which could disrupt the intermolecular π-π stacking of the phenylalanine residues at the positions 19 and 20 of the Aβ42. To enhance the inhibitory activity of BSBps against the Aβ42 aggregation, we designed and synthesized a series of β-strand-fixed peptides (BSFps) whose side chains are cross-linked.

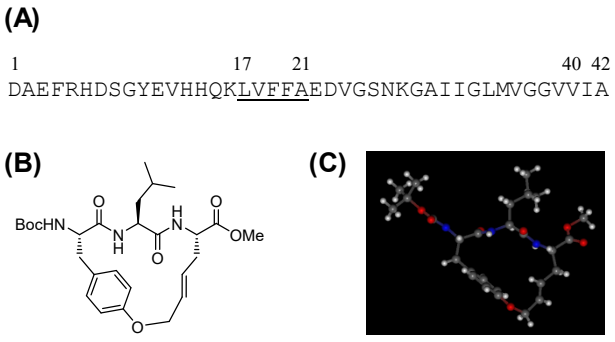

Figure 1. (A) Amino acid sequence of Aβ42. 'LVFFA' region is underlined. Chemical structure (B) and X-ray crystal structure (C) of a β-strand-fixed tripeptide developed by Abell *et al*.[27]

2. Results

*2.1. BSFps with Abell's motif (**1**–**4**)*

*2.1.1. Design and synthesis of **1**–**4***

$A\beta_{17–21}$ (LVFFA) pentapeptide was chosen as a template for designing the BSFps to target the core β-sheet structure in the central region of the Aβ42 aggregates (Figure 1A). In a general structural model of the β-strands, the side chains of neighboring residues face in the opposite directions, resulting in the same direction of every second side chain. Hence, we designed an $A\beta_{17–21}$-based pentapeptide **1** (Figure 2), in which, the side chains of 2nd and 4th residues were cross-linked by RCM to mimic the β-strand conformation using the Abell's motif (Figure 1B and 1C).[26, 27] Since the incorporation of Asp and Pro into BSBp could enhance their inhibitory activity,[13, 14] **2**–**4**, bearing Asp and/or Pro residues at the termini, were also designed (Figure 2).

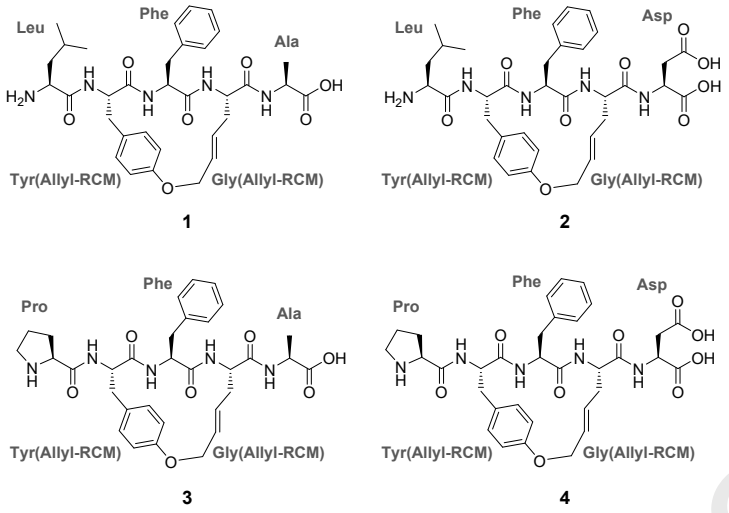

Figure 2. Chemical structures of **1**–**4**.

Our preliminary synthetic study found that the side-chain cross-linking of the peptides in the early-stage lead to low yield because the cross-linked peptides are poorly soluble in any solvent. Therefore, synthesis of **1**–**4** was conducted by solution-phase peptide elongation followed by ring-closing metathesis of dienes (Scheme 1). The starting material **5** (Boc-Tyr (Allyl)-OMe) was prepared as reported previously.[28] After alkaline hydrolysis of the methyl ester **5**, the resultant carboxylic acid was coupled with H-Phe-OMe using 1-[Bis(dimethylamino)methylene]-1*H*-benzotriazolium 3-Oxide Hexafluorophosphate (HBTU) and *N,N*-diisopropylethylamine (DIEA) to give dipeptide **6**. Hydrolysis of the methyl ester in **6** and the subsequent coupling with H-Gly(Allyl)-OMe provided tripeptide **7**, which can be used as a common synthetic intermediate for the syntheses of **1**–**4**. After hydrolysis of the methyl ester in **7**, the resultant carboxylic acid was condensed with H-Ala-OMe and H-Asp(OMe)-OMe to form tetrapeptide **8a** and **8b**, respectively. After removal of Boc groups from **8a** and **8b**, the resultant amines were acylated with Boc-Leu-OH and Boc-Pro-OH to give pentapeptides **9a**–**9d**. RCM of dienes **9a**–**9d** using Hoveyda-Grubbs' 2nd generation catalyst under high dilution condition resulted in **10a**–**10d** in high yields. (*E*)-configurations

of **10a**–**10d** were confirmed by the characteristic coupling constants (>15 Hz for trans) of the corresponding two vinylic protons. Few (*Z*)-isomers were detected in all the RCM products. In Abell's synthesis of β-strand-fixed tripeptide (Figure 1B), 10mol% Grubbs' 2nd generation catalyst was used for RCM of the dienes in 1,1,2-trichloroethane under thermal or microwave heating.[26, 27] They also reported that the addition of chlorodicyclohexylborane as Lewis acid markedly improved the yield of the RCM.[27] In contrast, we succeeded in high-yield RCM of the dienes **9a**–**9d** using 5mol% of Hoveyda-Grubbs' 2nd generation catalyst without additive in dichloromethane under reflux condition. Finally, hydrolysis of the methyl esters and subsequent removal of the Boc groups from **10a**–**10d** provided the desired **1**–**4**.

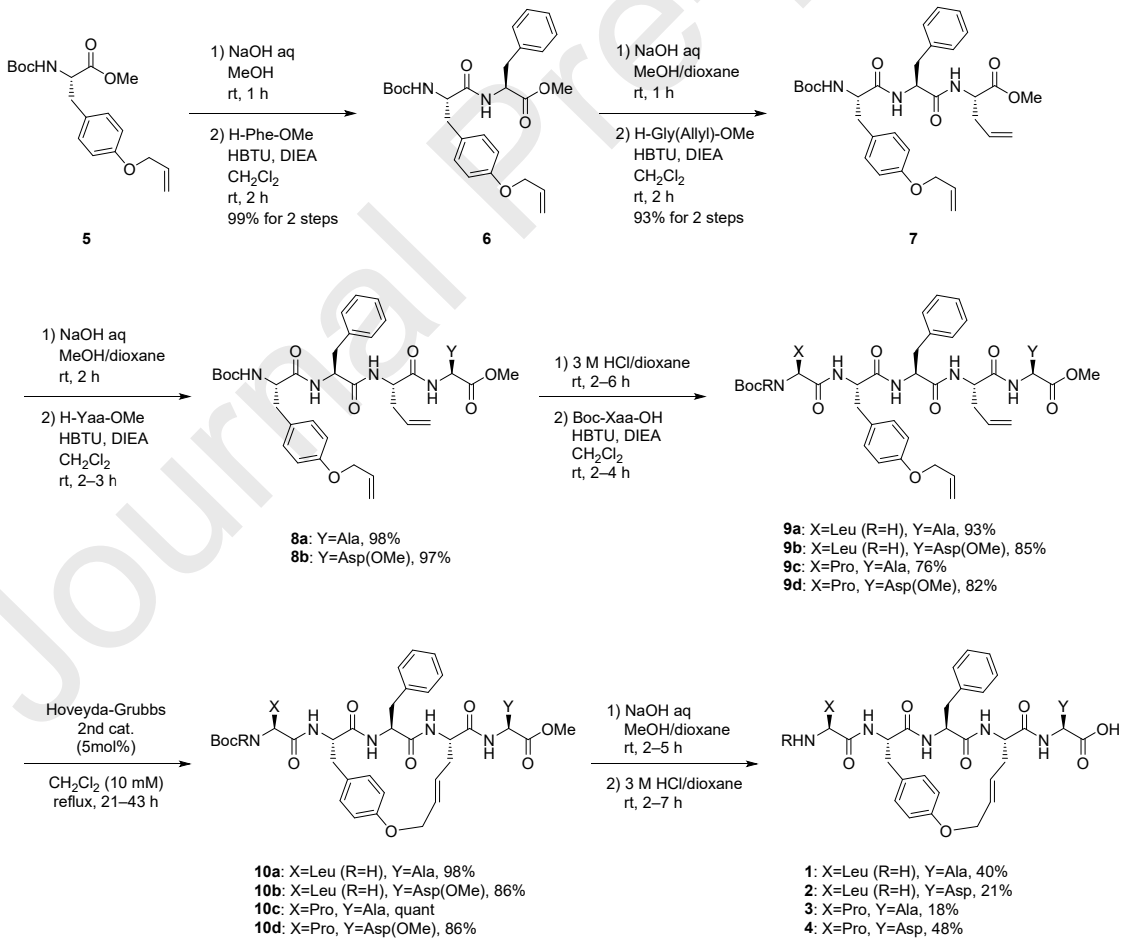

Scheme 1. Synthesis of **1**–**4**

*2.1.2. Conformational analysis of **1**–**4***

To verify whether the conformations of **1**–**4** were fixed to β-strand, their 3D structures were analyzed by NMR. NMR experiments for structural analysis were performed using dimethyl sulfoxide (DMSO)-d_6 as the solvent because all the BSFps were soluble in it. Since 2D NOESY experiments did not indicate any nuclear Overhauser effect (NOE) that can be used for distance information, dihedral angle information based on *J*-coupling constants between vicinal protons was used for conformation analysis. It has been reported that the amide proton-C_α proton coupling constants ($^3J_{HN\alpha}$) in the peptides and proteins correlate well with their torsion angles θ.[29, 30] Since dihedral angles ϕ of the peptides and proteins are dependent on the torsion angles θ, $^3J_{HN\alpha}$ is known to correlate with the local conformation; $^3J_{HN\alpha}$ value is typically 8–10 Hz for a β-strand conformation, 6–8 Hz for a random coil, and less than 6 Hz for an α-helix. $^3J_{HN\alpha}$ values of **1**–**4** were measured by 1D and 2D NMR experiments, which are summarized in Table 1. It is noteworthy that all the $^3J_{HN\alpha}$ values at the 4th residues (Gly(Allyl-RCM)) were considerably larger than 8 Hz, suggesting the formation of β-strand conformation at this position of **1**–**4**. On the other hand, $^3J_{HN\alpha}$ values at the 2nd, 3rd, and 5th residues were 6–8 Hz, indicating that these positions might not be fully fixed to the β-strand conformation.

3D structures of **1**–**4** were estimated by the molecular mechanics calculation on CONFLEX 8 program.[31-33] Molecular modelling was performed using the distance geometry followed by a conformational search based on the reservoir-filling algorithm with dihedral angle constraints derived from the NMR data. The θ-angles at the 4th residues of **1**–**4** were set at around 180°, which constrain the position in a β-strand conformation. Since the $^3J_{HN\alpha}$ values of 6–8 Hz can be observed in any conformations, the θ-angles at the 2nd, 3rd, and 5th residues were not constrained for the calculations. The search limit was set at 3 kcal/mol

above the global energy minimum. For energy minimization, we applied MMFF94s force field with a dielectric constant value of 46.45 (the dielectric constant for DMSO at 25 °C).

The above calculations yielded stable conformations of **1**–**4** as shown in Figure 3. The ϕ and ψ angles of the lowest energy conformers (Figures 3A, C, E, and G) are summarized in Table S1. It is well known that the amino acid with torsion angles in the range of $-180° < \phi < -45°$ and $45° < \psi < 225°$ are considered to be in the β-sheet region.[34, 35] According to this empirical rule, the ϕ and ψ angles of **1**–**4** (Table S1) suggested that all the residues form a β-strand conformation. The similarity of the macrocyclic frames in the superpositions of the top-10 stable conformers (Fig. 3B, D, F, and H) supported their rigidity.

Table 1. $^3J_{HN\alpha}$ (Hz) values for **1**–**4** in DMSO-d_6 at 25 °C.

Compound	Residue No.	Residue	$^3J_{HN\alpha}$ (Hz)
1	1	Leu	N.D.[a]
	2	Tyr(Allyl-RCM)[b]	7.1
	3	Phe	6.8
	4	Gly(Allyl-RCM)[b]	9.2
	5	Ala	7.2
2	1	Leu	N.D.[a]
	2	Tyr(Allyl-RCM)[b]	7.3
	3	Phe	6.7
	4	Gly(Allyl-RCM)[b]	9.2
	5	Asp	6.0
3	1	Pro	N.D.[a]
	2	Tyr(Allyl-RCM)[b]	7.1
	3	Phe	6.9
	4	Gly(Allyl-RCM)[b]	9.1
	5	Ala	7.0
4	1	Pro	N.D.[a]
	2	Tyr(Allyl-RCM)[b]	7.0
	3	Phe	7.0
	4	Gly(Allyl-RCM)[b]	9.0
	5	Asp	7.9

[a]The $^3J_{HN\alpha}$ values for the 1st residues could not be determined.

[b]The side chains of the residues were cross-linked by RCM (see Figure 2).

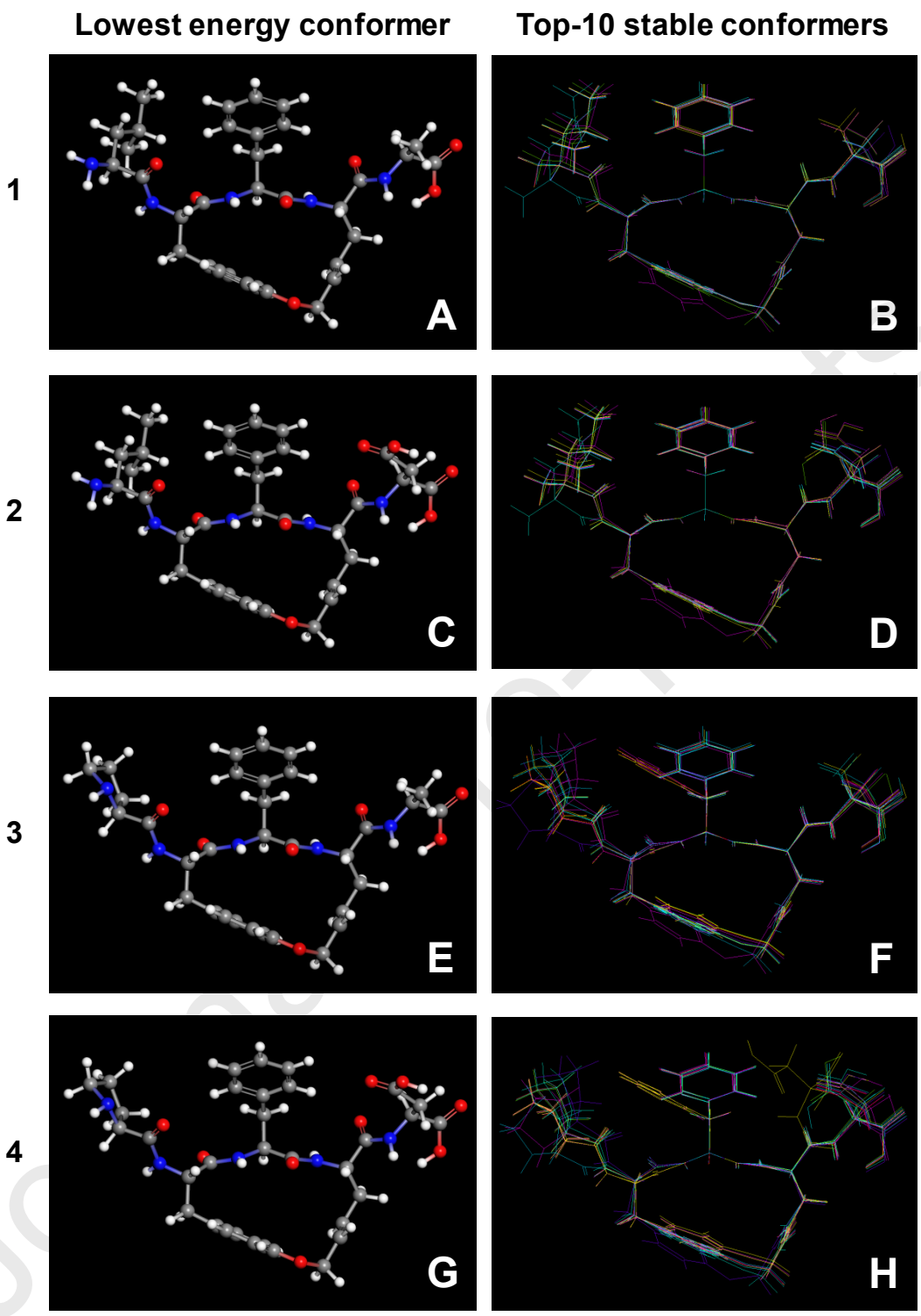

Figure 3. 3D structural models of **1** (A, B), **2** (C, D), **3** (E, F), and **4** (G, H) proposed by the molecular mechanics calculations with restrained conformational search by the distance geometry method. The lowest energy conformers (A, C, E, and G) and superposition of the top-10 stable conformers (B, D, F, and H) of **1**–**4** are shown. The ϕ and ψ angles of the lowest energy conformers (Figures 3A, C, E, and G) are summarized in Table S1.

*2.1.3. Effect of **1**–**4** on Aβ42 aggregation*

Inhibitory activities of **1**–**4** against Aβ42 aggregation were evaluated by using thioflavin-T (Th-T), which detects the Aβ42 aggregates through fluorescence.[36] For comparison, the activities of linear peptides such as LVFFA and LPFFD were also analyzed. As shown in Figure 4A, only **1** among all the peptides significantly reduced the relative Th-T fluorescence caused by Aβ42 aggregation. We confirmed that **1** exhibited dose-dependent inhibition of Th-T fluorescence by Aβ42 aggregation (Figure S1). These data indicated the potent inhibition of Aβ42 aggregation by **1**. On the other hand, the Th-T fluorescence was only slightly decreased by LVFFA and LPFFD. These data suggested that the cross-linking of the side chains could enhance the inhibitory activity of BSBps against the Aβ42 aggregation. Since the inhibition of the Th-T fluorescence by **2**–**4** was weaker than that of **1**, introduction of Pro and/or Asp residue into the termini of BSFps would decrease the inhibitory activities.

To analyze the effect of BSFps on the fibril formation of Aβ42, we observed the morphology of the Aβ42 aggregate co-incubated with each peptide for 48 h using transmission electron microscopy (TEM) (Figure 5). Since all the aggregates were found to form fibril structures, **1**–**4** would not change the pathway of amyloid fibril formation.

*2.1.4. Effect of **1**–**4** on Aβ42-induced neurotoxicity*

Inhibitory activities of **1**–**4** against Aβ42-induced neurotoxicity were evaluated by MTT (3-(4,5-dimethylthiazol-2-yl)-2,5-diphenyltetrazolium bromide) assay using human neuroblastoma SH-SY5Y cells. After 48-h incubation of the cells with Aβ42 in the presence or absence of each compound, the viabilities of the resultant cells were evaluated by MTT assay. The cell viabilities with **1**–**4**, despite the 10-fold addition, were almost same as that without compound, indicating that not all the peptides prevented the Aβ42-induced toxicity significantly (Figure 4B and S2).

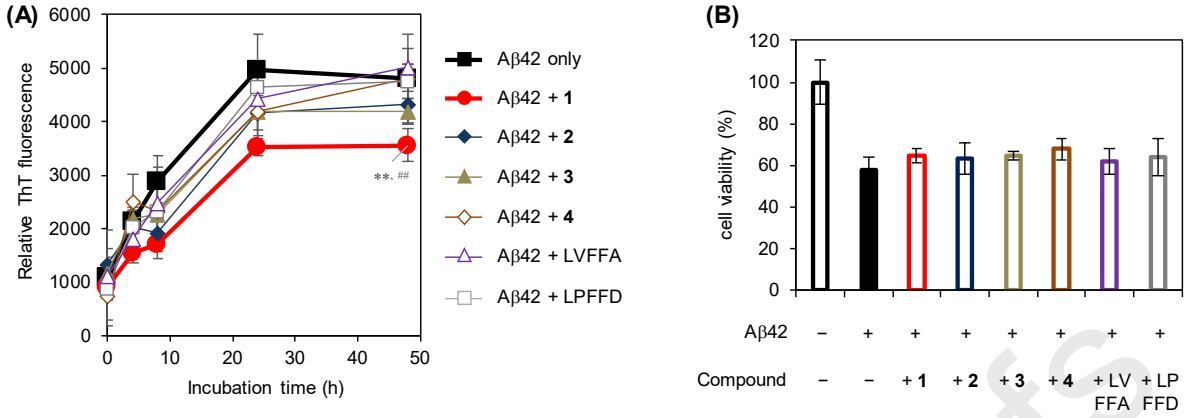

Figure 4. (A) Effect of **1**–**4** on the Aβ42 aggregation evaluated by Th-T assay (excitation: 430 nm, emission: 510 nm). Aβ42 (10 μM) was co-incubated with or without each compound (40 μM) in PBS (pH 7.4) at 37 °C. Data are presented as the mean ± SD (n = 4). ** $p < 0.01$ vs. Aβ42 only, ## $p < 0.01$ vs. Aβ42+LVFFA by Tukey-Kramer test. (B) Effect of **1**–**4** on Aβ42-induced toxicity in SH-SY5Y cells. After 48-h incubation of the cells with Aβ42 (1 μM) in the presence of each compound (10 μM), the viabilities of the resultant cells were evaluated by MTT assay. Data are presented as the mean ± SD (n = 3).

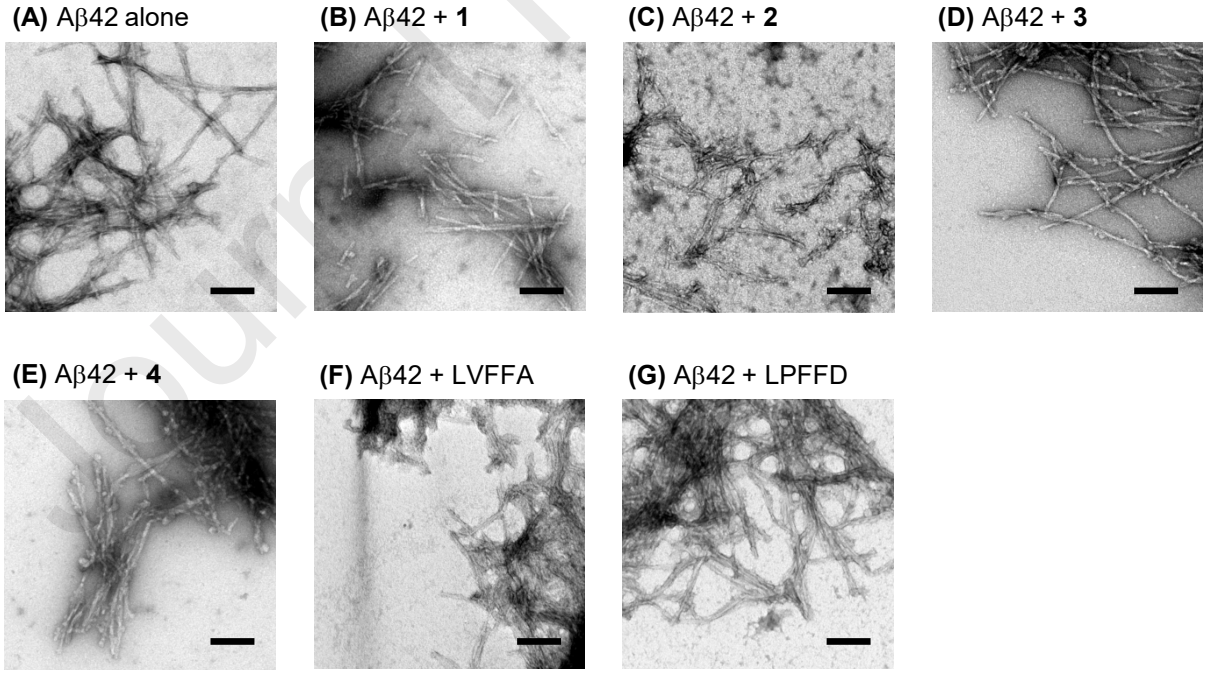

Figure 5. TEM images of Aβ42 aggregates prepared in the presence of BSFps **1**–**4**. The aggregates were prepared by incubation of Aβ42 (10 μM) with each compound (40 μM) in PBS (pH 7.4) at 37 ºC for 48 h. *Scale bar* = 100 nm.

*2.2. BSFps with various cross-linking motifs (**11**–**13**)*

*2.2.1. Design and synthesis of **11**–**13***

The study of **1**–**4** indicated that cross-linking of the side chains in BSFp pentapeptides could mimic the β-strand conformation and enhance their inhibitory activity against the Aβ42 aggregation. To find the optimal way of cross-linking, we designed and synthesized **11**–**13** whose cross-linking patterns were different from that of **1**–**4** (Figure 6). In these pentapeptides, the aromatic rings were located at the side chains of 3rd and 4th residues, mimicking the two successive phenylalanines of the LVFFA sequence. It should be noted that the positions of Tyr(Allyl-RCM) and Gly(Allyl-RCM) in **11** and **12** are opposite to those in Abell's motif (**1**–**4** and **13**). **11**–**13** were synthesized in the synthetic routes similar to those of **1**–**4** (Schemes S1–S3).

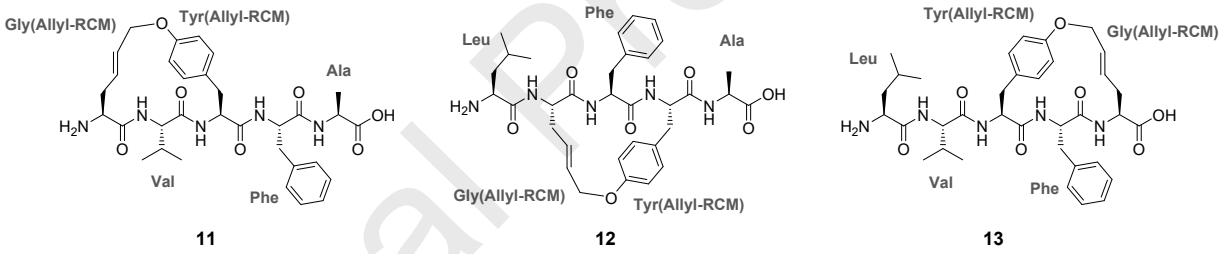

Figure 6. Chemical structures of **11**–**13**

*2.2.2. Conformational analysis of **11**–**13***

NMR analyses of **11**–**13** in DMSO-d_6 were performed and the obtained $^3J_{HN\alpha}$ values are shown in Table 2. The $^3J_{HN\alpha}$ values at 2nd and 3rd residues of **11** and those at 3rd and 4th residues of **12** were considerably larger than 8 Hz, suggesting the formation of β-strand at these positions.[29, 30] $^3J_{HN\alpha}$ value at 5th residue of **13** was 9.0 Hz, which is as large as at 4th residues of **1**–**4** (Table 1).

Molecular modelling of **11**–**13** was conducted in the same manner as those of **1**–**4**. The θ-angles with their $^3J_{HN\alpha}$ values larger than 8.5 Hz were set at around 180°. The obtained structural models are described in Figure 7, and ϕ and ψ angles of the lowest energy conformers (Figures 7A, C, and E) are summarized in Table S1. According to the empirical rule,[34, 35] the ϕ and ψ angles in the macrocyclic frames suggested that the residues are included in a β-strand conformation. Macrocyclic frames of the top-10 stable conformers were similar to each other, whereas two residues outside the macrocycles were quite different among the conformers (Figures 7B, D, and F).

Table 2. $^3J_{HN\alpha}$ (Hz) values for **11**–**13** in DMSO-d_6 at 25 °C.

Compound	Residue No.	Residue	$^3J_{HN\alpha}$ (Hz)
11	1	Gly(Allyl-RCM)[b]	N.D.[a]
	2	Val	9.0
	3	Tyr(Allyl-RCM)[b]	9.7
	4	Phe	8.0
	5	Ala	7.2
12	1	Leu	N.D.[a]
	2	Gly(Allyl-RCM)[b]	8.0
	3	Phe	8.6
	4	Tyr(Allyl-RCM)[b]	9.7
	5	Ala	6.9
13	1	Leu	N.D.[a]
	2	Val	8.7
	3	Tyr(Allyl-RCM)[b]	6.8
	4	Phe	6.5
	5	Gly(Allyl-RCM)[b]	9.0

[a]The $^3J_{HN\alpha}$ values for the 1st residues could not be determined.

[b]The side chains of the residues were cross-linked by RCM (see Figure 5).

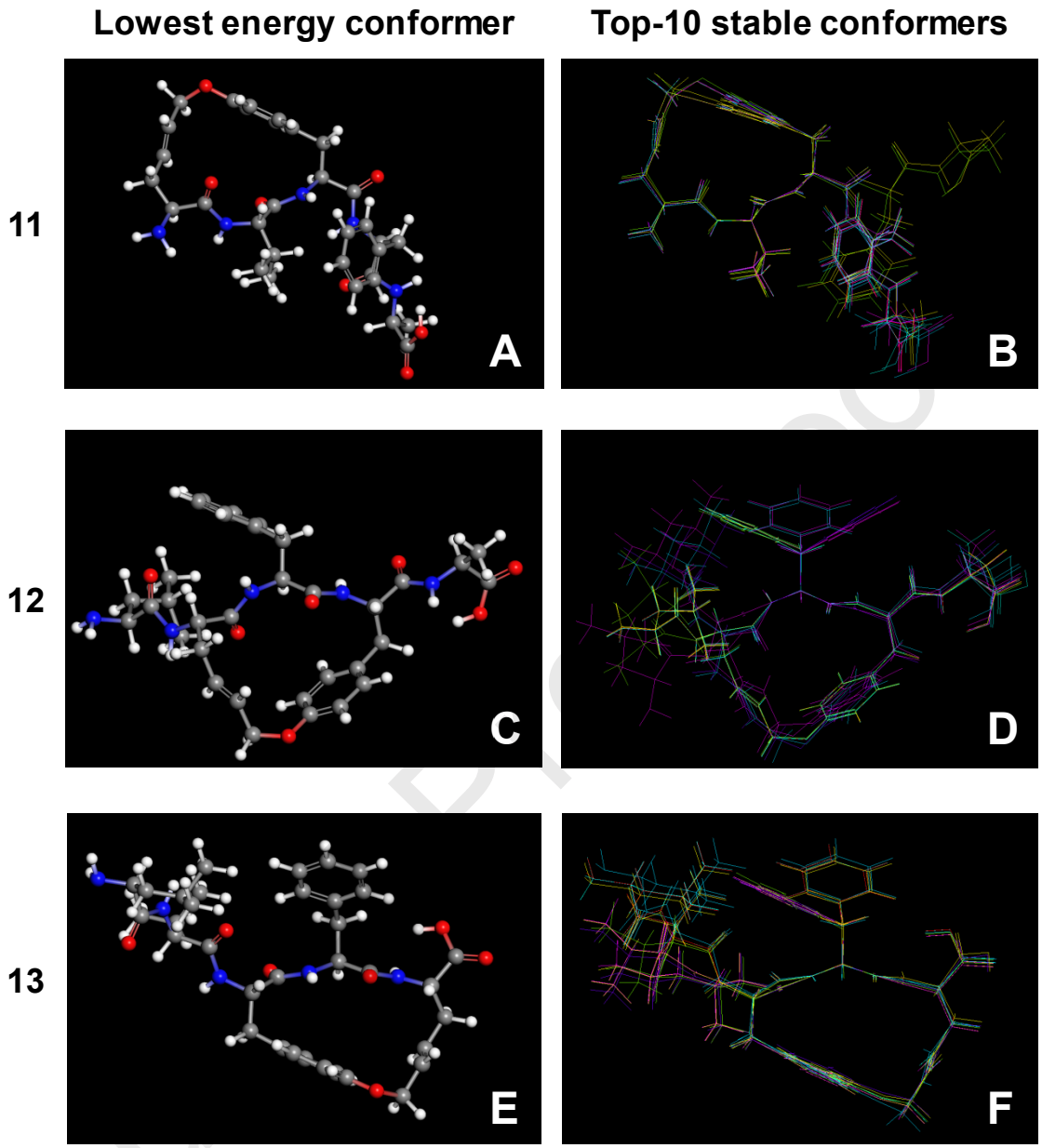

Figure 7. 3D structural models of **11** (A, B), **12** (C, D), and **13** (E, F) proposed by the molecular mechanics calculations with restrained conformational search by the distance geometry method. The lowest energy conformers (A, C, and E) and superposition of top-10 stable conformers (B, D, and F) of **11**–**13** are shown. The ϕ and ψ angles of the lowest energy conformers are summarized in Table S1.

*2.2.3. Effect of **11**–**13** on Aβ42 aggregation*

Inhibition of Aβ42 aggregation by **11**–**13** was evaluated using Th-T assay. **12** significantly decreased the relative Th-T fluorescence induced by the Aβ42 aggregation (Figure 8A) and the inhibitory activity was found to be dose-dependent (Figure S1), suggesting the potent inhibition of Aβ42 aggregation by **12**. However, the inhibitory activity of **12** was slightly weaker than that of **1**. In addition, incubation of **12** alone in PBS caused a slight increase of Th-T fluorescence (Figure S1), indicating a small amount of self-aggregation of **12**. On the other hand, **11** and **13** did not reduce the Th-T fluorescence, suggesting that these peptides could not inhibit the Aβ42 aggregation. TEM analysis of the Aβ42 aggregate co-incubated with each peptide suggested the formation of fibril structures in all the aggregates (Figure 9).

*2.2.4. Effect of **11**–**13** on Aβ42-induced neurotoxicity*

Effects of **11**–**13** on Aβ42-induced neurotoxicity were evaluated by MTT assay using SH-SY5Y cells. Since the cell viabilities in the presence of each compound were almost same as that without compound, **11**–**13** would not prevent the Aβ42-induced toxicity (Figure 8B). We confirmed that **12** alone exhibited significant toxicity against the cells (Figure S2). This cytotoxicity might be caused by the self-aggregation of **12** observed in the Th-T assay (Figure S1).

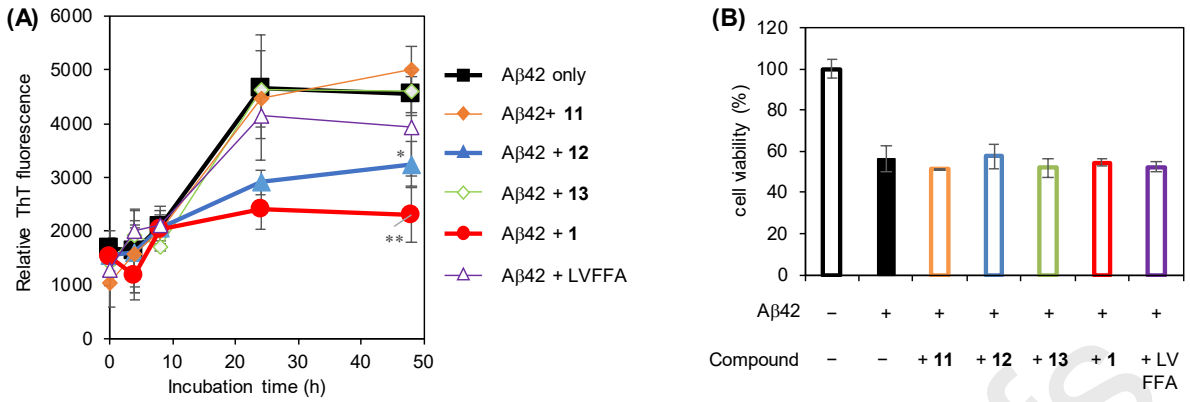

Figure 8. (A) Effect of **11**–**13** on Aβ42 aggregation evaluated by Th-T assay (excitation: 430 nm, emission: 510 nm). Aβ42 (10 μM) was co-incubated with or without each compound (40 μM) in PBS (pH 7.4) at 37 °C. Data are presented as the mean ± SD (n = 4). ** $p < 0.01$ vs. Aβ42 only. (B) Effect of **11**–**13** on Aβ42-induced toxicity in SH-SY5Y cells. After 48-h incubation of the cells with Aβ42 (1 μM) in the presence of each compound (10 μM), the viabilities of the resultant cells were evaluated by MTT assay. Data are presented as the mean ± SD (n = 3).

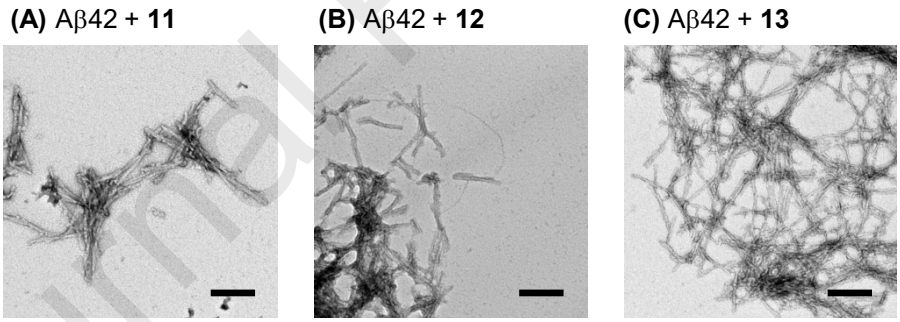

Figure 9. TEM images of Aβ42 aggregates prepared in the presence of BSFps **11**–**13**. The aggregates were prepared by incubation of Aβ42 (10 μM) with each compound (40 μM) in PBS (pH 7.4) at 37 ºC for 48 h. *Scale bar* = 100 nm.

3. Discussion

3.1. Verification of β-strand-fixation by cross-linking of side chains

In this study, we synthesized two types of BSFps: 'Tyr(Allyl-RCM)-Xaa-Gly(Allyl-RCM)' such as **1**–**4** and **13**, and 'Gly(Allyl-RCM)-Xaa-Tyr(Allyl-RCM)' such as **11** and **12**. As shown in Tables 1 and 2, $^{3}J_{HN\alpha}$ values for Gly(Allyl-RCM) in 'Tyr(Allyl-RCM)-Xaa-Gly(Allyl-RCM)' type and those for Tyr(Allyl-RCM) in 'Gly(Allyl-RCM)-Xaa-Tyr(Allyl-RCM)' type were much larger than 8.0 Hz. This indicated that the designed motifs could fix the residues in the β-strand conformation. It is noteworthy that the $^{3}J_{HN\alpha}$ values of Xaa in the 'Gly(Allyl-RCM)-Xaa-Tyr(Allyl-RCM)' type (**11** and **12**) were considerably large. The motif might strongly fix the conformation of this residue in β-strand.

Our conformational analysis proposed 3D structural models of the synthesized peptides (Figures 3 and 7). 3D structures of the macrocyclic frames of **1**–**4** were quite similar to that in the X-ray crystal structure of Abell's tripeptide (Figure 1C).[27] This supports the validity of our methodology for conformational analysis. The ϕ and ψ angles of the lowest energy structures (Table S1) indicated that three residues in the macrocycle (2nd to 4th residues in **1**–**4** and **12**, 1st to 3rd residues in **11**, and 3rd to 5th residues in **13**) should form the β-strand conformation. Although the side chains and two successive residues were variable, the macrocyclic frames of top-10 stable conformers were similar in each compound. These data strongly supported that the cross-linking of the side chains in every second residue is an effective way to fix the peptide conformation in a β-strand.

3.2. Structure-activity relationships of BSFp

1 and **12** inhibited the aggregation of Aβ42, whereas **11** and **13** did not (Figures 4A and 8A). As described above, the whole conformation of **1** and **12** were fixed to the β-strand, but

two residues outside the macrocycle were variable in **11** and **13** (Figures 3 and 7). The positions of cross-linking in the peptides should be critical for β-strand-fixation, leading to a high affinity to the β-sheet in the Aβ42 aggregates. Incorporation of Pro and/or Asp residues in the terminus did not enhance but reduce the inhibitory activity against the Aβ42 aggregation as shown in case of **2**–**4** (Figures 4A). Since LPFFD also did not prevent the aggregation, introduction of Pro and/or Asp residue might not enhance the inhibitory activity in Th-T assay. Murvai *et al.* indicated that LPFFD might interrupt the assembly of protofilaments.[37] This might be a reason why LPFFD would not alter the aggregation kinetics of Aβ42 in Th-T assay because binding of Th-T to the protofilament could also increase its fluorescence.

Although **1** and **12** inhibited the Aβ42 aggregation in Th-T assay (Figure 4A), these peptides could not prevent the Aβ-induced neurotoxicity in SH-SY5Y cells (Figure 4B). This might be due to their little effect on the aggregation pathway of Aβ42. Soluble Aβ aggregates formed in the pathway of amyloid fibrils are known to be toxic to neuronal cells.[38-40] The aggregation pathway could be changed into non-toxic by some aggregation inhibitors.[41, 42] Cyclic BSBp developed by Arai *et al.*[21,22] and Jha *et al.*[23] also prevented the formation of fibrillar aggregates, resulting in the reduction of Aβ-induced neuronal death. In contrast, our BSFp **1** and **12** could slow the aggregation kinetic (Figure 4A and 8A), but had little effect on the morphologies of the Aβ42 fibrils (Figure 5 and 9). This might be a reason why **1** and **12** could not alleviate the neurotoxicity of Aβ42 in SH-SY5Y cells. The difference of the experimental condition between Th-T assay and cell-based assay should be also considered. The content in the cell culture such as protein and cell membrane might interact with BSFp, leading to fewer interactions between BSFp and Aβ42 molecules.

4. Conclusion

In this study, we designed and synthesized a new type of BSBp whose side chains were cross-linked by RCM to fix the conformation in a β-strand. According to the conformation analysis, cross-linking of every second side chains could fix the conformation of peptides in the β-strands. Among the synthesized pentapeptides, **1** and **12**, whose side chains at the 2nd and 4th residues were cross-linked, inhibited the aggregation of Aβ42 in Th-T assay, suggesting that the β-strand conformation fixation of BSBp could improve their inhibitory activity against the Aβ42 aggregation. However, **1** and **12** could not change the aggregation state of Aβ42 into a nontoxic one.

5. Materials and methods

5.1. Molecular modeling based on NMR Data

General techniques of NMR experiments were described in Supplementary Material. $^{3}J_{HN\alpha}$ values in Tables 1 and 2 were determined by ^{1}H-1D along with ^{1}H-^{1}H *J*-resolved 2D and DQF-COSY experiments.

Molecular modeling was performed on the CONFLEX 8 program[31-33] by the distance geometry method. For energy minimization, we utilized MMFF94s force field with a dielectric constant value of 46.45 (DMSO at 25 °C). Conformational search was performed using the reservoir-filling algorithm with dihedral angle constraints derived from the NMR data (Tables 1 and 2); the θ-angles with their $^{3}J_{HN\alpha}$ values larger than 8.5 Hz were set at 180° with force constant of 1 kcal•mol^{-1}•rad^{-2}. The search limit was set at 3 kcal/mol above the global energy minimum. Atomic coordinates and calculated potential energies of the lowest-energy structures were described in Supplementary material.

5.2 Preparation of Aβ42

Aβ42 peptide was kindly provided by Prof. Kazuhiro Irie at Graduate School of Agriculture in Kyoto University. Synthetic procedure of the Aβ42 peptide was described elsewhere.[43, 44]

Aβ42 peptide for all the assays was pre-treated with 1,1,1,3,3,3-hexafluoro-2-propanol (HFIP) to dissociate aggregation seeds, which were unavoidably formed during purification and/or storage. Aβ42 peptide was dissolved in HFIP at 1 mg/mL. After being incubated at room temperature for 30 min, the solution was sonicated for 5 min, and dried in vacuo using a centrifugal evaporator. The resultant film (HFIP-treated Aβ42) was used for all the assays.

5.3. Thioflavin-T (Th-T) fluorescence assay

To 534 μL of phosphate buffered saline (PBS: 50 mM sodium phosphate with 100 mM NaCl, pH 7.12) was added 6 μL of each compound solution (4 mM in DMSO), then 60 μL of Aβ42 solution (100 μM in 0.1% NH_4OH). The final solution included 10 μM of Aβ42, 40 μM of each compound, and 1% DMSO in PBS (pH 7.4). After being incubated at 37 °C for 0, 4, 8, 24, 48 h, the suspension was vortexed for 5 second and 15 μL of the aliquot was collected in a 96-well black plate. The plate was stored at –80 °C until measurement.

To each well of the plate was added 235 μL of 5.0 μM Th-T in 50 mM Gly-NaOH (pH 8.5), followed by the measurement of fluorescence using a 430 nm (FWHM 10 nm) a excitation filter and a 510 nm (FWHM 40 nm) emission filter on a microplate reader (TriSter LB941, Berthold Technologies). The background of the buffer without Aβ42 was subtracted from recorded values.

5.4. Transmission electron microscopy (TEM)

Morphology of the Aβ42 aggregates co-incubated with each compound were observed by a TEM (Figures 5 and 9). The incubation conditions were the same as that for preparing the samples for the Th-T assay. A solution of Aβ42 (10 μM) and each compound (40 μM) in PBS (containing 1% DMSO, pH 7.4) was incubated at 37 °C for 48 h. After centrifugation, the supernatant was removed from the pellets, and the aggregates were suspended in distilled water by gentle vortex mixing. The suspensions were applied to a 200-mesh formvar-coated copper grid (Nissin EM, Tokyo, Japan) and allowed to stand for 5 min before being negatively stained with 2% uranylacetate. The fibrils were examined with the H-7650 electronmicroscope (Hitachi).

5.5. Cell culture

Human neuroblastoma SH-SY5Y cells were obtained from the American Type Culture Collection (ATCC®, CRL-2266™). They were cultured in Dulbecco's Modified Eagle Medium/F-12 Nutrient Mixture (Gibco) containing 10% (v/v) fetal bovine serum (Biowest), 100 U/mL penicillin, and 100 μg/mL streptomycin at 37 °C under 5% CO_2 atmosphere.

5.6. MTT assay

Near-confluent cultures of cells were plated at 2.0 × 10^4 cells/200 μL/well fresh culture medium in 96-well plates, and pre-incubated at 37 °C under 5% CO_2 for 24 h. To the cell culture was added 1 μL of compound solution (2.2 mM in DMSO) and 20 μL of Aβ42 solution (11 μM in 0.1% NH_4OH) and. The final culture included 10 μM of each compound, 1 μM of Aβ42, 0.5% DMSO, and 0.01% NH_4OH. After incubation at 37 °C under 5% CO_2 for 48 h, 20 μL of MTT solution (5 mg/mL in water) was added to each well, followed by incubation at 37 °C for 4 h. After discarding the medium, 100 μL of DMSO was added to each well. The optical density of the cell lysate was read at 545 nm (after background

subtraction at 630 nm) using a microplate reader (CHROMATE4300, Awareness Technology Inc.). The absorbance obtained by adding the vehicle was taken as 100%.

Acknowledgments

This research was supported by Sugiyama Houkoukai (grant in 2020). The authors are grateful to Prof. Kazuhiro Irie, Assoc. Prof. Kazuma Murakami, and Dr. Yumi Irie at Graduate School of Agriculture in Kyoto University for kindly providing Aβ42 peptides. The authors greatly thank Prof. Minoru Inagaki at Graduate School of Bioresources in Mie University for his generous support in the laboratory.

Supplementary Material

Figures S1−S2, Table S1, Schemes S1−S4, synthetic procedures (**1**−**4**, **11**−**13**, LVFFA, LPFFD), copies of ^{1}H and ^{13}C NMR spectra for synthetic compounds, and atomic coordinates and calculated potential energies of the lowest-energy structures. This material is available via the Internet.

References and notes

1. Selkoe DJ, Hardy J. The amyloid hypothesis of Alzheimer's disease at 25 years. *EMBO Mol Med*. Jun 2016;8(6):595-608. doi:10.15252/emmm.201606210

2. Glenner GG, Wong CW. Alzheimer's disease: initial report of the purification and characterization of a novel cerebrovascular amyloid protein. *Biochem Biophys Res Commun*. May 16 1984;120(3):885-90. doi:10.1016/s0006-291x(84)80190-4

3. Masters CL, Simms G, Weinman NA, Multhaup G, McDonald BL, Beyreuther K. Amyloid plaque core protein in Alzheimer disease and Down syndrome. *Proc Natl Acad Sci U S A*. Jun 1985;82(12):4245-9. doi:10.1073/pnas.82.12.4245

4. Crouch PJ, Harding SM, White AR, Camakaris J, Bush AI, Masters CL. Mechanisms of A beta mediated neurodegeneration in Alzheimer's disease. *Int J Biochem Cell Biol*. 2008;40(2):181-98. doi:10.1016/j.biocel.2007.07.013

5. Jarrett JT, Berger EP, Lansbury PT, Jr. The carboxy terminus of the beta amyloid protein is critical for the seeding of amyloid formation: implications for the pathogenesis of Alzheimer's disease. *Biochemistry*. May 11 1993;32(18):4693-7. doi:10.1021/bi00069a001

6. Meier BH, Riek R, Bockmann A. Emerging Structural Understanding of Amyloid Fibrils by Solid-State NMR. *Trends Biochem Sci*. Oct 2017;42(10):777-787. doi:10.1016/j.tibs.2017.08.001

7. Loquet A, El Mammeri N, Stanek J, et al. 3D structure determination of amyloid fibrils using solid-state NMR spectroscopy. *Methods*. Apr 1 2018;138-139:26-38. doi:10.1016/j.ymeth.2018.03.014

8. Serpell LC. Alzheimer's amyloid fibrils: structure and assembly. *Biochim Biophys Acta*. Jul 26 2000;1502(1):16-30. doi:10.1016/s0925-4439(00)00029-6

9. Antzutkin ON, Leapman RD, Balbach JJ, Tycko R. Supramolecular structural constraints on Alzheimer's beta-amyloid fibrils from electron microscopy and solid-state nuclear magnetic resonance. *Biochemistry*. Dec 24 2002;41(51):15436-50. doi:10.1021/bi0204185

10. Tycko R. Insights into the amyloid folding problem from solid-state NMR. *Biochemistry*. Mar 25 2003;42(11):3151-9. doi:10.1021/bi027378p

11. Gazit E. A possible role for pi-stacking in the self-assembly of amyloid fibrils. *Faseb j*. Jan 2002;16(1):77-83. doi:10.1096/fj.01-0442hyp

12. Porat Y, Abramowitz A, Gazit E. Inhibition of amyloid fibril formation by polyphenols: structural similarity and aromatic interactions as a common inhibition

mechanism. *Chem Biol Drug Des*. Jan 2006;67(1):27-37. doi:10.1111/j.1747-0285.2005.00318.x

13. Soto C, Kindy MS, Baumann M, Frangione B. Inhibition of Alzheimer's amyloidosis by peptides that prevent beta-sheet conformation. *Biochem Biophys Res Commun*. Sep 24 1996;226(3):672-80. doi:10.1006/bbrc.1996.1413

14. Soto C, Sigurdsson EM, Morelli L, Kumar RA, Castano EM, Frangione B. Beta-sheet breaker peptides inhibit fibrillogenesis in a rat brain model of amyloidosis: implications for Alzheimer's therapy. *Nat Med*. Jul 1998;4(7):822-6. doi:10.1038/nm0798-822

15. Tjernberg LO, Naslund J, Lindqvist F, et al. Arrest of beta-amyloid fibril formation by a pentapeptide ligand. *J Biol Chem*. Apr 12 1996;271(15):8545-8. doi:10.1074/jbc.271.15.8545

16. Austen BM, Paleologou KE, Ali SA, Qureshi MM, Allsop D, El-Agnaf OM. Designing peptide inhibitors for oligomerization and toxicity of Alzheimer's beta-amyloid peptide. *Biochemistry*. Feb 19 2008;47(7):1984-92. doi:10.1021/bi701415b

17. Adessi C, Frossard MJ, Boissard C, et al. Pharmacological profiles of peptide drug candidates for the treatment of Alzheimer's disease. *J Biol Chem*. Apr 18 2003;278(16):13905-11. doi:10.1074/jbc.M211976200

18. Cruz M, Tusell JM, Grillo-Bosch D, et al. Inhibition of beta-amyloid toxicity by short peptides containing N-methyl amino acids. *J Pept Res*. Mar 2004;63(3):324-8. doi:10.1111/j.1399-3011.2004.00156.x

19. Chalifour RJ, McLaughlin RW, Lavoie L, et al. Stereoselective interactions of peptide inhibitors with the beta-amyloid peptide. *J Biol Chem*. Sep 12 2003;278(37):34874-81. doi:10.1074/jbc.M212694200

20. Francioso A, Punzi P, Boffi A, et al. beta-sheet interfering molecules acting against beta-amyloid aggregation and fibrillogenesis. *Bioorg Med Chem*. Apr 15 2015;23(8):1671-83. doi:10.1016/j.bmc.2015.02.041

21. Arai T, Araya T, Sasaki D, et al. Rational design and identification of a non-peptidic aggregation inhibitor of amyloid-beta based on a pharmacophore motif obtained from cyclo[-Lys-Leu-Val-Phe-Phe-]. *Angew Chem Int Ed Engl*. Jul 28 2014;53(31):8236-9. doi:10.1002/anie.201405109

22. Arai T, Sasaki D, Araya T, Sato T, Sohma Y, Kanai M. A cyclic KLVFF-derived peptide aggregation inhibitor induces the formation of less-toxic off-pathway amyloid-beta oligomers. *Chembiochem*. Nov 24 2014;15(17):2577-83. doi:10.1002/cbic.201402430

23. Jha A, Kumar MG, Gopi HN, Paknikar KM. Inhibition of beta-Amyloid Aggregation through a Designed beta-Hairpin Peptide. *Langmuir*. Jan 30 2018;34(4):1591-1600. doi:10.1021/acs.langmuir.7b03617

24. Loughlin WA, Tyndall JD, Glenn MP, Fairlie DP. Beta-strand mimetics. *Chem Rev*. Dec 2004;104(12):6085-117. doi:10.1021/cr040648k

25. Loughlin WA, Tyndall JD, Glenn MP, Hill TA, Fairlie DP. Update 1 of: Beta-strand mimetics. *Chem Rev*. Jun 9 2010;110(6):Pr32-69. doi:10.1021/cr900395y

26. Abell AD, Jones MA, Coxon JM, et al. Molecular modeling, synthesis, and biological evaluation of macrocyclic calpain inhibitors. *Angew Chem Int Ed Engl*. 2009;48(8):1455-8. doi:10.1002/anie.200805014

27. Abell AD, Alexander NA, Aitken SG, et al. Synthesis of Macrocyclic β-Strand Templates by Ring Closing Metathesis. *The Journal of Organic Chemistry*. 2009/06/05 2009;74(11):4354-4356. doi:10.1021/jo802723w

28. Roosenburg S, Laverman P, Joosten L, et al. Stabilized (111)in-labeled sCCK8 analogues for targeting CCK2-receptor positive tumors: synthesis and evaluation. *Bioconjug Chem*. Apr 21 2010;21(4):663-70. doi:10.1021/bc900465y

29. Pardi A, Billeter M, Wuthrich K. Calibration of the angular dependence of the amide proton-C alpha proton coupling constants, 3JHN alpha, in a globular protein. Use of 3JHN alpha for identification of helical secondary structure. *J Mol Biol*. Dec 15 1984;180(3):741-51. doi:10.1016/0022-2836(84)90035-4

30. Smith LJ, Bolin KA, Schwalbe H, MacArthur MW, Thornton JM, Dobson CM. Analysis of main chain torsion angles in proteins: prediction of NMR coupling constants for native and random coil conformations. *J Mol Biol*. Jan 26 1996;255(3):494-506. doi:10.1006/jmbi.1996.0041

31. Goto H, Osawa E. Corner flapping: a simple and fast algorithm for exhaustive generation of ring conformations. *Journal of the American Chemical Society*. 1989/11/01 1989;111(24):8950-8951. doi:10.1021/ja00206a046

32. Gotō H, Ōsawa E. An efficient algorithm for searching low-energy conformers of cyclic and acyclic molecules. 10.1039/P29930000187. *Journal of the Chemical Society, Perkin Transactions 2*. 1993;(2):187-198. doi:10.1039/P29930000187

33. CONFLEX 8. Goto, H. Obata, S. Nakayama, N. Ohta, K. *CONFLEX Corporation, Tokyo, Japan, 2017*.

34. Ramachandran GN, Ramakrishnan C, Sasisekharan V. Stereochemistry of polypeptide chain configurations. *Journal of Molecular Biology*. 1963/07/01/ 1963;7(1):95-99. doi:https://doi.org/10.1016/S0022-2836(63)80023-6

35. Hovmoller S, Zhou T, Ohlson T. Conformations of amino acids in proteins. *Acta Crystallogr D Biol Crystallogr*. May 2002;58(Pt 5):768-76. doi:10.1107/s0907444902003359

36. Naiki H, Gejyo F. [20] Kinetic analysis of amyloid fibril formation. *Methods in Enzymology*. Academic Press; 1999:305-318.

37. Murvai Ü, Soós K, Penke B, Kellermayer MSZ. Effect of the beta-sheet-breaker peptide LPFFD on oriented network of amyloid β25-35 fibrils. *Journal of Molecular Recognition*. 2011/05/01 2011;24(3):453-460. doi:10.1002/jmr.1113

38. Nichols MR, Colvin BA, Hood EA, Paranjape GS, Osborn DC, Terrill-Usery SE. Biophysical comparison of soluble amyloid-beta(1-42) protofibrils, oligomers, and protofilaments. *Biochemistry*. Apr 7 2015;54(13):2193-204. doi:10.1021/bi500957g

39. Walsh DM, Hartley DM, Kusumoto Y, et al. Amyloid beta-protein fibrillogenesis. Structure and biological activity of protofibrillar intermediates. *J Biol Chem*. Sep 3 1999;274(36):25945-52. doi:10.1074/jbc.274.36.25945

40. Shankar GM, Li S, Mehta TH, et al. Amyloid-beta protein dimers isolated directly from Alzheimer's brains impair synaptic plasticity and memory. *Nat Med*. Aug 2008;14(8):837-42. doi:10.1038/nm1782

41. Ladiwala AR, Lin JC, Bale SS, et al. Resveratrol selectively remodels soluble oligomers and fibrils of amyloid Abeta into off-pathway conformers. *J Biol Chem*. Jul 30 2010;285(31):24228-37. doi:10.1074/jbc.M110.133108

42. Ehrnhoefer DE, Bieschke J, Boeddrich A, et al. EGCG redirects amyloidogenic polypeptides into unstructured, off-pathway oligomers. *Nat Struct Mol Biol*. Jun 2008;15(6):558-66. doi:10.1038/nsmb.1437

43. Irie K, Oie K, Nakahara A, et al. Molecular Basis for Protein Kinase C Isozyme-Selective Binding: The Synthesis, Folding, and Phorbol Ester Binding of the Cysteine-Rich Domains of All Protein Kinase C Isozymes. *Journal of the American Chemical Society*. 1998/09/01 1998;120(36):9159-9167. doi:10.1021/ja981087f

44. Murakami K, Irie K, Morimoto A, et al. Synthesis, aggregation, neurotoxicity, and secondary structure of various A beta 1-42 mutants of familial Alzheimer's disease at positions 21-23. *Biochem Biophys Res Commun*. May 31 2002;294(1):5-10. doi:10.1016/s0006-291x(02)00430-8

Graphical abstract